International Journal of Bridge Engineering (IJBE), Special Issue 2016, pp. 135-162

SHAKE TABLE STUDIES OF A PRECAST BRIDGE PIER WITH ADVANCED MATERIALS

Sarira Motaref[1], M. Saiid Saiidi[2], David Sanders[3], Amir Mirmiran[4]

[1] Assistant Professor in Residence, University of Connecticut, Dept. of Civil and Environmental Engineering, 261 Glenbrook Rd., Unit 3037, Storrs, CT 06269, USA.
[2, 3] Professor, University of Nevada, Reno, Department of Civil and Environmental Engineering Mail Stop 258, Reno, NV 89557, USA.
[4] Provost and Vice President for Academic Affairs, Professor and Lindsey Chair of Civil Engineering, The University of Texas at Tyler 3900 University Blvd., Tyler, TX 75799.
e-mail: motaref@engr.uconn.edu, saiidi@unr.edu, sanders@unr.edu, amirmiran@uttyler.edu

ABSTRACT: An experimental and analytical study was conducted on the seismic performance of a 0.3-scale two-column bent incorporating two precast columns with advanced materials, a precast footing, and a precast cap beam. The objective was to determine if the connection details and construction methods used in this study are appropriate for accelerated bridge construction (ABC) in high seismic zones and if using advanced materials can reduce the earthquake damage compared to conventional reinforced concrete columns. One column was built using conventional reinforced concrete, but incorporated ECC (engineered cementitious composite) in the plastic hinge zone instead of concrete. The other column consisted of a glass fiber reinforced polymer tube filled with concrete. Two pockets were formed in the footing to allow for insertion of precast columns. The column embedment length was designed to transfer the full plastic moment of the column to the footing. The column-pier cap connection was a telescopic steel pipe pin adapted for ABC. The pier model was subjected to the Sylmar earthquake record simulated on a shake table with increasing amplitudes until failure. Test results showed that the seismic performance of both columns was satisfactory and that the embedment length was sufficient to develop the plastic moment in both columns. A comprehensive analytical model of the pier was developed using OpenSEES and acceptable correlation was obtained between the measured and calculated data. Parametric studies were conducted to determine the effect of variables that were not included in the experimental studies.

KEYWORDS: Accelerated bridge construction, Seismic Performance, Precast, Shake Table, ECC, CFFT, Pipe-Pin Hinges

1 INTRODUCTION

Conventional bridge construction is time consuming causing possible traffic

delays. In contrast, prefabricated bridge elements can be built concurrently, thus allowing for accelerated bridge construction (ABC) and minimizing interruption to the highway network.

Precast reinforced concrete (RC) columns meeting seismic design requirements were used in the State of Washington for ABC ([1]). Hieber, et al., [2] studied a cast-in-place (CIP) pier system and a hybrid pier system incorporating precast concrete columns, a precast beam, and a cast in place foundation and found that behavior of these piers was similar to conventional cast-in-place pier behavior. Conventional reinforced concrete was used in these studies.

As an alternative to RC columns, FRP (fiber reinforced polymer) tubes filled with concrete could be considered. FRP tube can act as a light-weight permanent formwork in construction of concrete columns in buildings or as piles and piers in bridges. The tube eliminates the time and labor for traditional formwork and its removal. The tube also acts as a life-long protective jacket for concrete core in hostile environments. Extensive studies in the past decade have shown satisfactory performance with respect to ductility capacity and damage of cast-in-place CFFT (concrete filled FRP tube) elements because the high tensile strength of FRP is mobilized in combination with the high compressive strength of confined concrete ([3], [4], [5], [6]). The performance of precast CFFT columns for ABC in high seismic zones has not been studied.

ABC provides an opportunity to further improve the seismic performance of RC bridge columns by utilizing innovative materials such as ECC (engineered cementitious composite) in plastic hinge zones of columns while minimizing damage. ECC displays a relatively high tensile strain capacity, tensile strain hardening, and energy dissipation compared to ordinary concrete and many other fiber-reinforced concrete materials ([7], [8], [9]). ECC has the ability to reach ultimate tensile strain of approximately 3% to 5% ([10]). This high strain capacity is nearly 500 times larger than that of conventional concrete.

Connection of precast columns to the pier cap and footing is critical particularly under seismic loading. One method is to leave a pocket in the footing or the cap beam, insert the precast column, and fill the gap with a grout. Such pocket must be of sufficient depth to allow for development of the column plastic moment. Variables such as column axial load, load eccentricity, shape of embedded members, and effective width of member should be considered in design of column embedded length [11]. Pertold, et al., [12] proposed a design model for embedded steel columns to transfer moment, shear, and axial load in the connection using plastic stress distribution analysis. Sadeghian and Fam [13] suggested an embedment length equal to 70% of the CFFT column diameter to achieve simultaneous material failure of the CFFT outside the footing and bond failure inside the footing.

Another method to connect columns to footings or pier caps is to use steel pipe pins to provide two-way hinge connections ([14]). Past research has

demonstrated satisfactory seismic performance of these connections in CIP construction and has led to development of seismic design guidelines for pipe pins at top of columns. There are other instances in which steel pipes have been utilized to transfer shear forces between concrete members as shear connectors ([15], [16]; [17]; [18]; [19]). In all the aforementioned applications, the pipe is subjected to shear with only minor rotation, whereas in column hinges, significant relative rotation is anticipated at the top of the columns under the lateral loads attributable to plastic hinging of the column base.

2 RESEARCH OBJECTIVE

The primary purpose of this study was to investigate several novel concepts integrated in a two-column bent consisting of precast elements to resist strong earthquake loading while minimizing damage. A two-column pier model was designed and tested on one of the shake tables at the University of Nevada, Reno.

One column was a CFFT element and the other was a conventional RC element except that concrete in the plastic hinge was replaced with ECC. In this paper the former column is referred to as "CFFT" and the latter is referred to as "RC-ECC." Both columns utilized steel pipe-pin connections to a precast cap beam and were embedded in pre-existing pockets in a precast footing to provide moment connections. Additional objectives of the study were to evaluate the performance and design of the column embedment length for CFFT and RC-ECC, pipe pins in precast construction, and ECC plastic hinges. Furthermore, to help understand the behavior of the model and evaluate the adequacy of analytical techniques, computer program OpenSEES was used to study the test model and conduct parametric studies.

3 TEST MODEL

A 0.3-scale precast two-column pier, PFEB (precast FRP-ECC bent) was studied. Three innovative details were used in the pier: ECC in the plastic hinge zone of one of the columns, CFFT in the other column, and steel pipe pins at top of both columns. The two-column test model provided the opportunity to study two different column types under the same lateral displacements demand while the connection details to cap beam and footing were identical in both columns. Pipe-pin hinges provide a moment free connection between the columns and the cap beams. It was assumed that both columns are cantilever and plastic hinge develops at lower part of columns. To measure the base shears in each of the columns, a load cell was placed in the middle of the cap beam.

Figure 1 shows the overall dimensions and details of the model. The diameter of RC-ECC and nominal diameter of CFFT was 355-mm (14-in.). ECC was placed over a 610-mm (24-in.) part of RC-ECC in the plastic hinge zone that was calculated by Eq. (1), [20] and considering the factor of safety of

2. This length was from 76-mm (3-in.) below the footing top surface to 533-mm (21-in.) above the footing (*Fig. 1*).

$$L_p = 0.08 \times H_c + 0.15 \times d_b \times f_y (\text{ksi})$$
$$L_p = 0.08 \times H_c + 0.022 \times d_b \times f_y (MPa) \quad (1)$$

Where: L_p is Plastic hinge length,

H_c is column height,

d_b is the diameter of longitudinal reinforcement,

f_y is the steel yield stress.

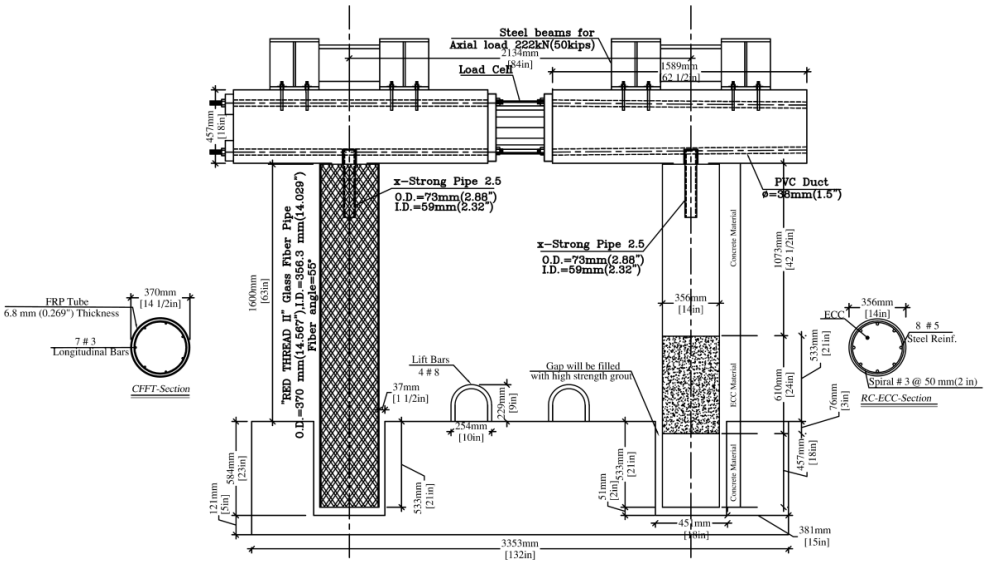

Figure 1. PEFB bent detail

The FRP tube wall thickness was 6.83-mm (0.269-in.), with glass fibers at +/- 55° providing strength in the longitudinal and hoop directions of the column. The longitudinal steel ratio in RC-ECC and CFFT was 1.60% and 0.46%, respectively. The effective longitudinal reinforcement ratio in CFFT was 0.78%. The equivalent FRP reinforcement ratio is calculated based on the cross sectional area of the tube, as converted to an equivalent area of steel based on the strength of Grade 60 steel, or simply $\rho f_y / f_u$, where ρ =reinforcement ratio of the FRP tube and f_y and f_u are yield strength of steel and ultimate strength of FRP, respectively ([21]). A model for the longitudinal behavior of the FRP tube was used to conduct moment-curvature analysis ([4]). More details about the test model are provided in ([22]).

3.1 Design of the test model

It was assumed that the pier is part of a bridge built in high seismic zones. The Caltrans provisions were used to design the transverse reinforcement in RC-ECC for a displacement ductility capacity of five for the column ([23]). This results in a volumetric steel ratio of 1.48%.

The cap beam and the footing were designed to remain elastic. Two pockets were left in the footing to provide space for anchoring the columns. The depth of the pocket was 584-mm (23-in.), which was equal to 1.50 times the column diameter plus 50-mm (2-in.) gap underneath of column. A load cell was incorporated in the cap beam to help determine shear in each column.

3.2 Column embedment length design

The column embedment length in the footing was designed so that full moment capacity of the column can be developed at the top of the footing. *Figure 2* shows the axial load, shear, bending moment and simplified stress distribution in the column footing connection ([24]). A study by Petrold, et al., [24] showed that the concrete stress in the horizontal direction can be set to 0.67 f_c' to account for the orientation of the principal stresses not being horizontal.

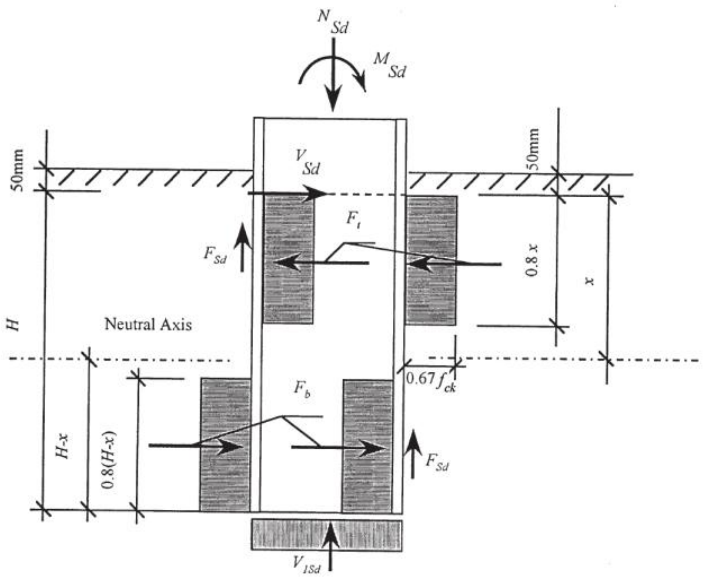

Figure 2. Stress distribution in column base [24] with permission

Taking the moments about the bottom of the column, the following equation was:

$$M_{Sd} + V_{Sd}H + F_b 0.4(H - x) - F_t(H - 0.4x) = 0 \qquad (2)$$

Where: V_{sd} is the maximum shear acting at bottom of the column,

M_{sd} is the maximum moment acting at bottom of the column,

F_t is the horizontal forces at the top,

F_b is the horizontal forces at the bottom transmitted from the column to the concrete.

These forces is calculated as

$$F_t = 0.8x0.67\, f_c' b_{eff}$$
$$F_b = 0.8(H - x)0.67\, f_c' b_{eff} \quad (3)$$

Using horizontal equilibrium, the neutral axis location is derived as

$$x = \frac{0.93V_{Sd} + 0.5 b_{eff}\, f_c' H}{b_{eff}\, f_c'} \quad (4)$$

Combining Eqs.(2) to (4), the embedded length H of the column is calculated as:

$$H = \frac{1.56V_{Sd} + \sqrt{4.74V_{sd}{}^2 + 6.22M_{Sd}\, f_c' b_{eff}}}{b_{eff}\, f_c'} \quad (5)$$

Where: f_c' is the concrete compressive strength,

b_{eff} is the effective width of the column Eq.(6) based on equivalent square area.

$$b_{eff} = \sqrt{\pi}\,\frac{D}{2} \quad (6)$$

Where: D is the column diameter

Pertold et al., [12] showed that the required embedment length H is typically between the effective width and twice the effective width and recommended the latter length.

To design the embedment length, the maximum plastic moment of the section and plastic shear of the column were calculated using specified material properties. The embedded length in the current study was calculated based on Eq.5 and was increased by 25% to 1.5 D to be conservative.

3.3 Pipe pin design

The pipe pins were designed to remain elastic using a procedure developed by Zaghi et al., [25]. This method accounts for different modes of failure consisting of concrete bearing against the pipe, diagonal tension in the column, and pure shear of the pipe. The ultimate lateral load capacity at the interface accounts for

reduction due to the impact resulting from the slippage between the column and the superstructure after the friction capacity at the interface is exceeded.

3.4 Material properties

Bars #3 were used as longitudinal reinforcement in CFFT and transverse reinforcement in RC-ECC , and #5 bars were used as longitudinal reinforcement in RC-ECC. The specified and measured yield strengths of steel reinforcement are listed in Table 1.

Table 1. Material Properties for Steel Reinforcement

Type	Diameter, in (mm)	Design yield strength, Ksi, (Mpa)	Measured yield strength, Ksi, (Mpa)	Ultimate yield strength, Ksi, (Mpa)
#3	0.375 (9.52)	60 (414)	67 (466)	105.7 (728)
#5	0.625 (15.87)	60 (414)	80 (551)	105 (724)

Table 2 lists the specified and measured compressive strength of ECC and concrete used in columns construction. The volume fraction of fiber in ECC was 2%. ASTM Type I/II Portland cement and FT Bridger fly ash were used. The fibers in ECC were expected to provide some confinement. However, the lateral reinforcement was designed to provide full confinement treating ECC as regular concrete. A high strength, fast-setting grout (SPEED-E-ROC) was used to fill the gap between the column and the footing. Compressive strength of grout is listed in Table 2. The material properties for FRP tube were based on the supplier technical information (Table 3.).

Table 2. Compressive Strengths of Concrete, Engineered Cementitious Composite, and Grout

Columns	Location	Design compressive strength ksi (MPa)	Strength ksi (MPa)	
			28 Days	Test Day
RC-ECC	Footing and Top part of Column	5.0 (34.5)	4.28 (29.5)	5.25 (36.2)
CFFT	Inside the FRP Tube	5.0 (34.5)	4.79 (33)	5.68 (39.2)
RC-ECC	ECC in Plastic Hinge	5.0 (34.5)	5.22 (36)	5.61 (38.7)
Bent	Grout between columns-Footing	5.0 (34.5)	6.41 (44.2)	7.05 (48.6)

Table 3. Mechanical Properties of FRP Tube

Property	ksi (MPa)
Axial tensile ultimate stress	10.3 (71)
Axial tensile modules of elasticity	1820 (12548)
Axial compressive ultimate stress	33 (230)
Axial compressive modules of elasticity	8687 (1260)
Beam bending ultimate stress	23 (158.6)
Beam bending modules of elasticity	1460 (10000)
Ultimate hoop tensile stress	34 (234)
Hoop tensile modules of elasticity	2180 (15030)

3.5 Construction

Construction of PEFB included building all the precast members and assembling the bent. The steel pipes at the pipe-hinge connections were filled with concrete and instrumented with strain gauges (*Fig. 3*).

Figure 3. Pipe-pin hinge detail

The concrete in the footing and the upper part of RC-ECC was cast first followed by casting of ECC. The concrete in CFFT and the rest of RC-ECC was cast last. Assembling the bent included inserting the columns into the footing holes, and filling the gap with grout (*Fig. 4*). The cap beam was then placed on the top of the columns (*Fig. 5*). Finally high strength-fast setting grout was cast and filled the space between the column and the footing pockets. PEFB was assembled in approximately three hours.

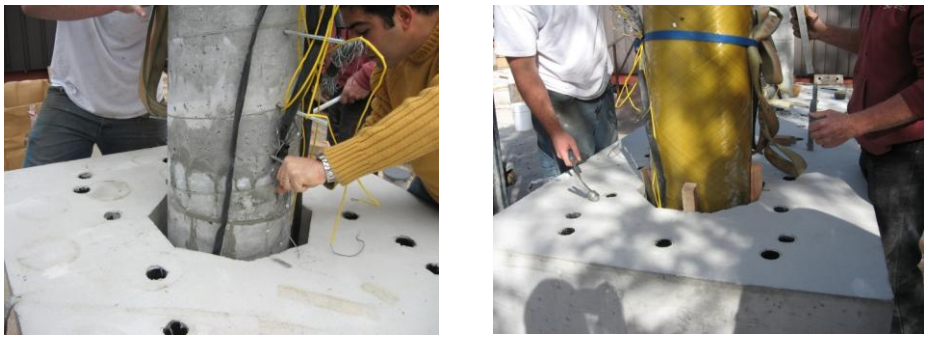

(a) (b)

Figure 4. Inserting the columns into the footing a) in RC-ECC, b) in CFFT

Figure 5. Cap beam installation

4 TEST SETUP AND LOADING PROTOCOL

The test model was attached rigidly to a shake table and a mass rig link (*Fig. 6*). To provide greater safety and the ability to test the specimens to complete failure, the axial loading system and the inertial mass were separated. The inertia mass was placed off the specimens for safety reason. The mass-rig consists of a four-hinge frame that is connected to the top of the column through a rigid link. The entire mass inertial forces are transmitted to the bent model.

Furthermore, the weight of the concrete blocks generates a P-Delta effect that is translated into additional shear on the bent. The total axial load on the bent was 356 kN (100 kips) and was applied using eight hydraulic jacks placed on the top of a steel spreader beams. The hydraulic system for these jacks was connected to an accumulator to minimize fluctuation of vertical load during shaking.

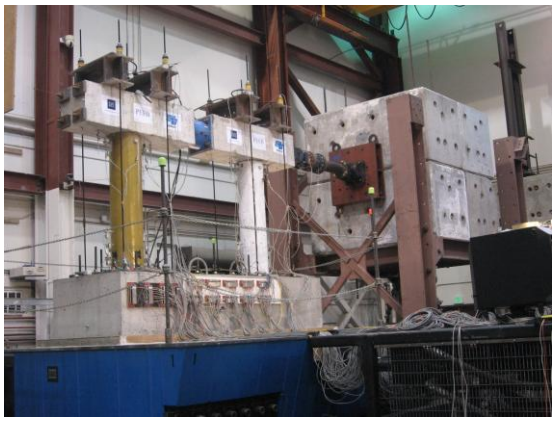

Figure 6. PEFB on the shake table

A large number of strain gages were placed on critical areas of steel reinforcement, pipe pins, and the FRP tube. In addition displacement transducers were installed at the top and bottom of the column to measure curvature, bond slip, relative slip between cap beam and column, and rotation. The lateral forces were measured using two load cells. One was embedded in the link assembly to measure the total lateral inertia force including the P-Delta effects generated by the mass rig. The second was a six-DOF load cell that was incorporated in the cap beam.

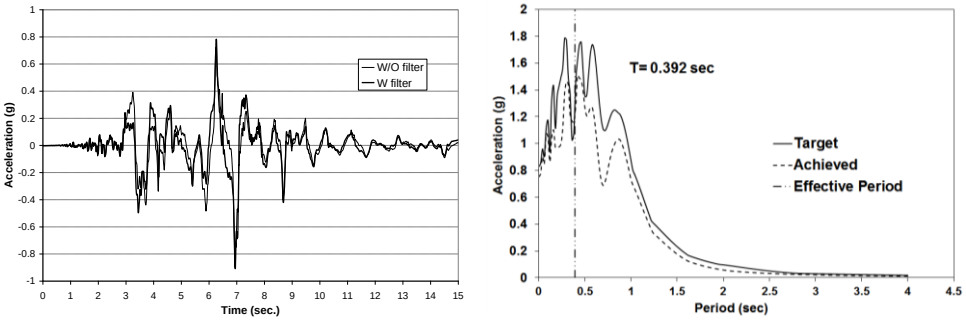

(a) (b)

Figure 7. a) Acceleration history of the ground motion, b) Target vs. achieved full Sylmar ground motion spectra

PEFB was subjected to a series of Sylmar ground motions (Northridge 1994) with the acceleration amplitude scaled by 0.1, 0.4, 0.7, 1, 1.3, and 1.65 in subsequent Runs. The full Sylmar motion had the maximum acceleration of 0.91g (*Fig.7 (a)*). The time coordinate of the input acceleration was compressed by a factor of $\sqrt{0.3} = 0.547$ to account for the scale of the test model, which

was 0.3. The testing was continued until failure of the test pier. *Fig. 7 (b)* shows the comparison of the pseudo acceleration spectra of the target motions versus the achieved shake table motions for full Sylmar ground motion. The natural period of the structure during this motion (1.0×Sylmar) is marked by the dashed line.

5 EXPERIMENTAL RESULTS

5.1 General observed performance

The column plastic hinges were expected to form at and near the base because the moment peaks at the column base. Flexural cracking at the bottom of RC-ECC was initiated during Run 2 and extended with minor ECC spalling observed after Run 4 (1×Sylmar).

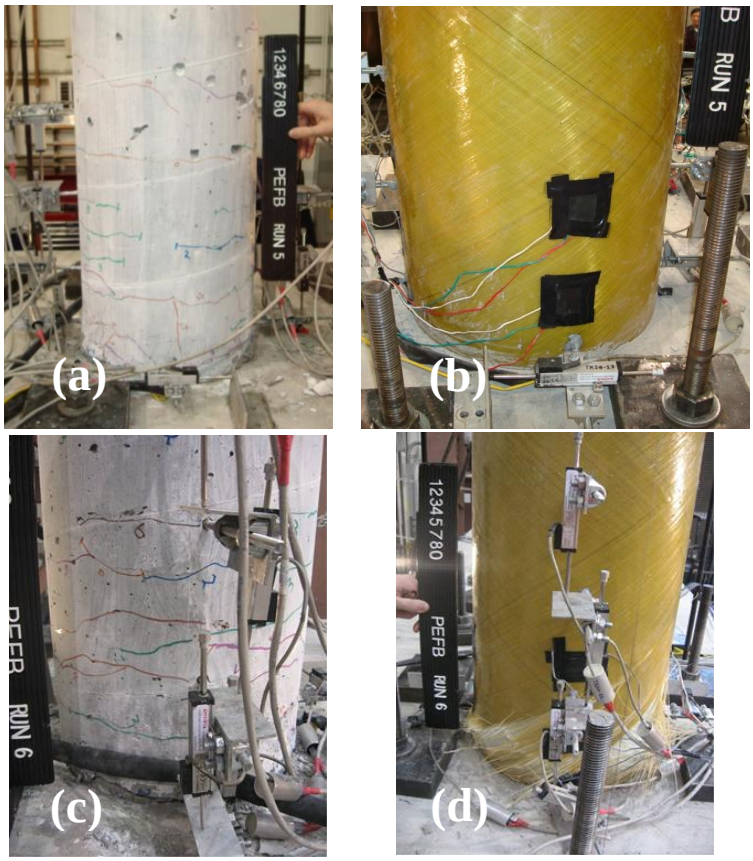

Figure 8. Damage progression photographs for a) RC-ECC, Run 5 b) CFFT, Run 5, c) RC-ECC, Run 6, d) CFFT, Run 6

Additional thin cracks were developed in the plastic hinge of RC-ECC during

Run 5 (*Fig. 8(a)*), but no damage could be observed in CFFT or connections (*Fig. 8(b)*). The maximum drift ratio under this Run was 8.6%, and yet there was no significant visible damage in the columns.

The columns failed during the last Run (1.65×Sylmar) at a drift ratio of 11.5% due to fracture of three bars in RC-ECC (*Figs. 8(c)* and *9(a)*) and rupture of fibers in CFFT (*Fig. 8(d*)). To investigate the condition of longitudinal bars within CFFT, the tube was removed after the test. It was found that two bars had buckled due to FRP rupture (*Fig. 9(b)*). No damage was noted in the pipe pins, thus demonstrating successful performance of these connections (*Fig. 10*).

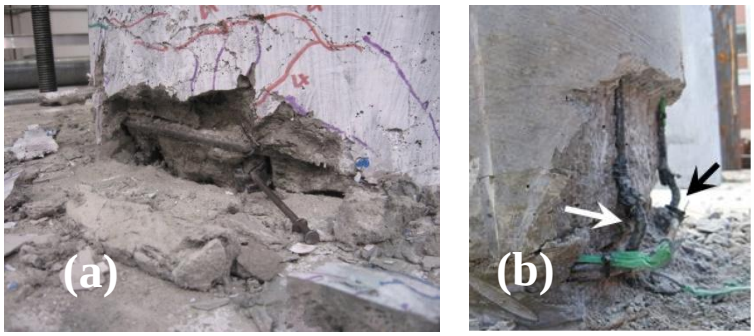

Figure 9. a) Rupture of longitudinal bars in RC-ECC, b) Buckled longitudinal bars in CFFT

Figure 10. Condition of the pipe pin after test

The maximum residual displacement ratios for the bent were plotted against the maximum displacement ratios in *Fig. 11*. It can be seen that residual displacements were less than 0.5%. The Japanese seismic design specifications for highway bridges limit residual drift ratio to 1% ([26]). Note that because of the coupling of the two columns through the cap beam, the residual displacement of the two column designs cannot be evaluated individually.

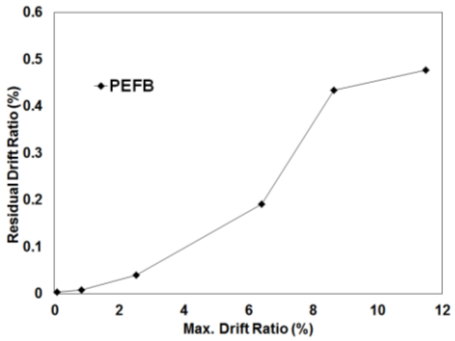

Figure 11. Residual drift ratios

The maximum measured base rotations in the RC-ECC and FRP columns during Run 5 (the run prior to the failure run causing a maximum drift ratio of approximately 8%) were 0.058 and 0.026 radians respectively. For approximately the same drift ratio, column rotations in a similar CIP bent were 0.04 and 0.025 radian, indicating that the precast bent essentially behaved the same as the CIP ([27]).

The bent damping ratios were calculated based on half-power bandwidth method and using the measured data from the white noise motions. The damping ratio measured after each earthquake run changed from 2 to 9% in the course of the testing. Contribution of FRP tube and ECC material in PEFB are believed to have caused this higher damping (up to 9%).

5.2 Force-displacement relationships

The horizontal displacement of the cap beam was the summation of the column displacement and the horizontal slippage at the pipe pins. The base shear of RC-ECC was obtained by subtracting the readings of the cap beam middle load cell from the link load cell data. Additional adjustments were made to account for the inertial forces attributable to the mass of the cap beam, steel loading beams, link, and other attachments. *Fig. 12* presents the measured force-displacement hysteresis curves of the bent, RC-ECC, and CFFT.

It can be seen that the hysteresis curves were relatively wide indicating high energy dissipation in each of the columns and the pier. The bold lines in these figures show the envelopes of the hysteresis curves. The maximum load in RC-ECC was 109.8 kN (24.7 kips) and it was recorded during Run 4 (1.0×Sylmar). The lateral load capacity in RC-ECC dropped by 46% to 59.1 kN (13.3 kips) during the last run after the plastic hinge failure. The maximum lateral load in CFFT was 149.9 kN (33.7 kips) dropping to 68.5 kN (15.4 kips) after failure, a 51 % loss.

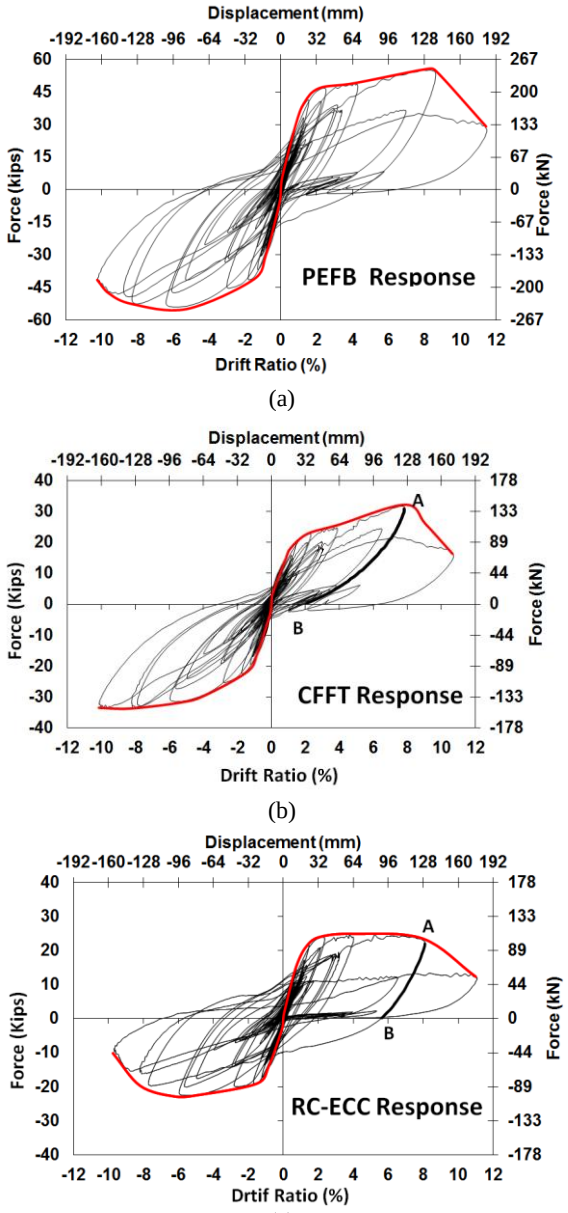

Figure 12. Load-displacement responses, a) PEFB Bent, b) CFFT, c) RC-ECC

The average envelopes of the measured hysteresis responses in the positive and negative displacement directions were used to compare the lateral load response of the columns (*Fig. 13 (a)*). The initial stiffness in the columns was the same, but the hardening after yielding was substantially more significant in CFFT

because the FRP tube remained elastic, while the steel reinforcing bars in RC-ECC yielded. The hardening of CFFT led to a peak lateral load that was 30% larger than RC-ECC capacity. The displacement ductility capacity of the columns was calculated from elasto-plastic idealizations of the envelopes using equal energy principle. The ductility capacity of RC-ECC was 7.8 compared to CFFT ductility capacity of 5.8. The lower ductility of CFFT is attributed to the higher load capacity and the larger effective yield displacement of CFFT. The failure displacement was the same in the two columns. But dividing the failure displacement by a larger yield displacement of CFFT resulted in a lower apparent ductility capacity. It should be noted that the drift capacity of both columns exceeded 11% indicating excellent performance.

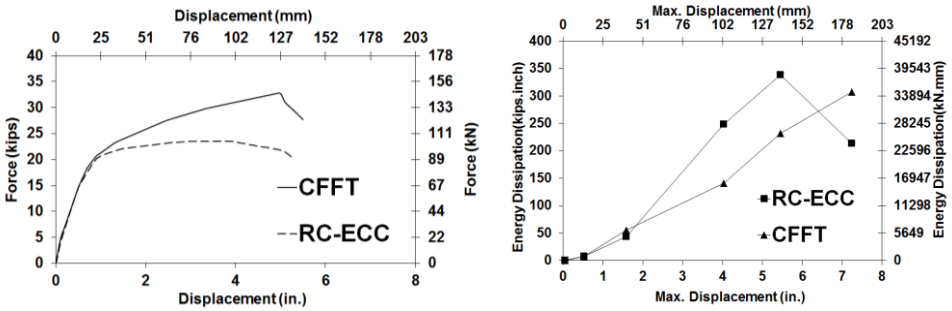

(a) (b)

Figure 13. a) Load-displacement responses, b) Columns energy dissipation

The dissipated energy was calculated by integrating the area enclosed by the force-displacement hysteretic curves. The dissipated energy versus the maximum displacement during each Run is plotted in *Fig. 13(b)*. It is evident that the energy dissipation was larger in RC-ECC in all the Runs except for the last Run when the bars ruptured. The larger energy dissipation in RC-ECC was attributed to the larger steel ratio and usage of ECC in its plastic hinge. The fact that the FRP tube remained elastic prior to failure resulted in sharper unloading slopes in the force displacement relationships (Segment AB in *Figs. 12(b)* and *12 (c)*). The sharper slope in *Fig. 12(b)* resulted in a smaller area within the hysteresis curves, hence lower energy dissipation in CFFT.

Table 4 lists the period of bent during each Run. The period of the bent increased from 0.278 second after the first run to 0.626 second after Run 6. The rupture of the FRP tube and longitudinal bars in RC-ECC column made the bent softer and led to these increased periods.

Table 4. Natural Periods of PEFB

Run	Period (second)
1	0.278
2	0.304
3	0.347
4	0.392
5	0.553
6	0.626

5.3 Strain data

Figure 14 shows the maximum and the minimum strain profiles of the outermost longitudinal bars for both columns. Positive strains denote tension and negative strains indicate compression. The measured yield strains for the bars in RC-ECC and CFFT were 3,600 μs and 3,200 μs , respectively. The figure reveals that most of the yielding in RC-ECC occurred at the bottom of the column. The maximum reliable measured strain of the longitudinal reinforcing bars in RC-ECC reached 106,656 μs during Run 4, which is approximately 29 times the yielding strain. The maximum strain of 200,000 μs in Fig. 14(a) is due to reaching the gage to its maximum measurement capacity or failure and coincided with the bar fracture at the foundation level in RC-ECC.

During Run 5 the maximum transverse bar strain in RC-ECC was 2,924 μs , which was 91% of the yield strain. The maximum strain in the transverse reinforcement in Run 6 (failure Run) was 3960 μs , which indicates limited yielding.

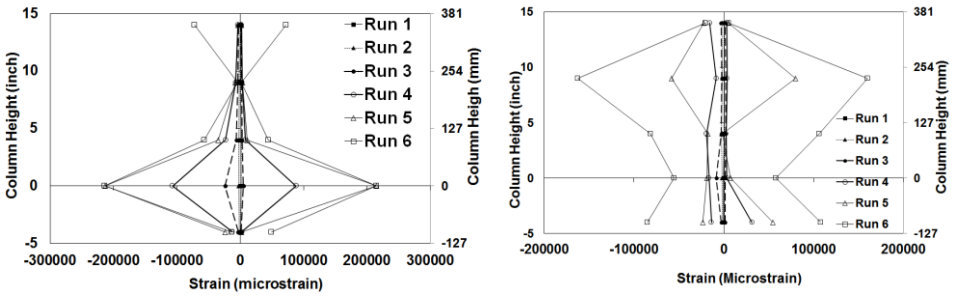

(a) (b)

Figure 14. The maximum and minimum long. strain profile of the a) RC-ECC, b) CFFT

The maximum strain of the longitudinal reinforcing bars in CFFT was 162,500 μs , which is approximately 50 times the measured yield strain. *Fig. 14(b)*

shows that the maximum strain occurred at 254-mm (10-in.) above the footing. The figure shows that the distribution of yielding is completely different from RC-ECC (*Fig. 14(a)*) and that plasticity is spread over a larger portion of the column length. This effect in FRP tube columns was also observed by Zhu et al., ([28]).

The yield stress in the steel pipe was 360 MPa (52.2 ksi) corresponding to strain of 1800 $\mu\varepsilon$. The maximum measured compressive strains were 4600 $\mu\varepsilon$ and 4200 $\mu\varepsilon$ in the pipe pins in RC-ECC and CFFT, respectively, which is approximately 2.5 times the yield strain. The extent of yielding was very limited and did not lead to permanent deformation of the pipes.

Two groups of strain gauges were installed on the FRP tube surface to measure the hoop and longitudinal strains. The hoop strain capacity of FRP tube is approximately 15,600 $\mu\varepsilon$. The maximum measured hoop strain reached 18,220 $\mu\varepsilon$ at 25-mm (1-in) above the footing level before failure. This strain was 16% larger than the ultimate capacity specified by the supplier and is consistent with the observed response.

5.4. Column-footing connections

To evaluate the novel column-footing connections used in this study, the PEFB results were compared to a similar test model, PPTC that was previously tested at UNR ([6]). The main differences between PPTC and PEFB were (1) The columns and footing were cast-in-place in PPTC, (2) the RC column in PPTC did not incorporate ECC, (3) the longitudinal steel in CFFT and RC in PPTC were 1.04% and 2.6%, respectively, whereas the steel ratio in CFFT and RC-ECC in PEFB were 0.46% and 1.6%, respectively. As a result, the lateral strength of PPTC was 53% higher than the strength of PEFB. The material properties in the two piers were comparable. The higher column longitudinal steel ratios in PPTC led to higher lateral load capacity compared to PEFB. It was therefore necessary to normalize the pushover curves for the two piers before their response could be compared. For each pier the lateral forces were normalized with respect to the measured force at 5% lateral drift ratio. The force at this drift level is a reasonable representation of the plastic load capacity. It can be seen in *Fig. 15* that the normalized pushover responses of two piers are closely correlated. The continued strain hardening beyond 89-mm (3.5-in) displacement in PPTC is due to the higher column longitudinal steel ratios in that pier. This demonstrates that precast construction can provide strengths and ductilities similar to those of comparable cast-in-place construction. The failure and extensive yielding of the columns at and near the base demonstrates that the column embedment lengths were sufficient in developing the full plastic moments and the connection performed as intended.

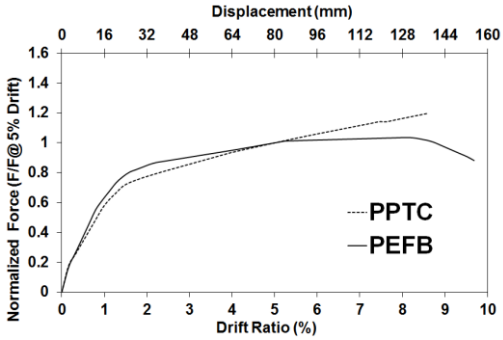

Figure 15. Comparison of backbone curves in PEFB and PPTC

5.5 Pipe pin connections

The hinge area of both columns after undergoing six Runs of a demanding earthquake was free from damage. This demonstrated successful performance of pipe-pin hinges in the construction. The bent was able to carry the vertical loads after the tests. The pipe-pin hinges remained essentially damage-free and were found to meet the performance objectives.

5.6 Comparison of damage in RC vs. RC-ECC columns

The comparisons of the apparent damage in RC column in PPTC (the cast in place bent tested by Zaghi et al., [6] and RC-ECC columns at different drift ratios are displayed in *Figs. 16*. The concrete cover in RC column spalled at 2% drift ratio (*Fig. 16(b)*). In contrast, RC-ECC cover was intact up to 6% drift ratio (*Fig. 16(c)*). ECC spalling in RC-ECC was minimal up to 11% drift ratio. However extensive concrete spalling was observed in RC column at 8% drift ratio (*Fig. 16(f)*). This indicates that the use of the ECC material in plastic hinge of RC-ECC helped minimizing damage. The damage was also more localized over a shorter height of the RC-ECC column.

6 ANALYTICAL STUDIES

6.1 Analytical model

The objective of the analytical studies was to determine the validity of the modeling assumptions based on the correlation between analytical and experimental results. Furthermore, upon establishing the reliability of analytical modeling method, the model was used to study several variations of the test model to determine the role of each parameter and find directions for optimal design of this type of precast construction. Optimal design in this study was defined as the optimum FRP tube thickness, FRP fiber orientation, and steel reinforcement ratio that result in the maximum lateral load capacity and the minimum residual displacement.

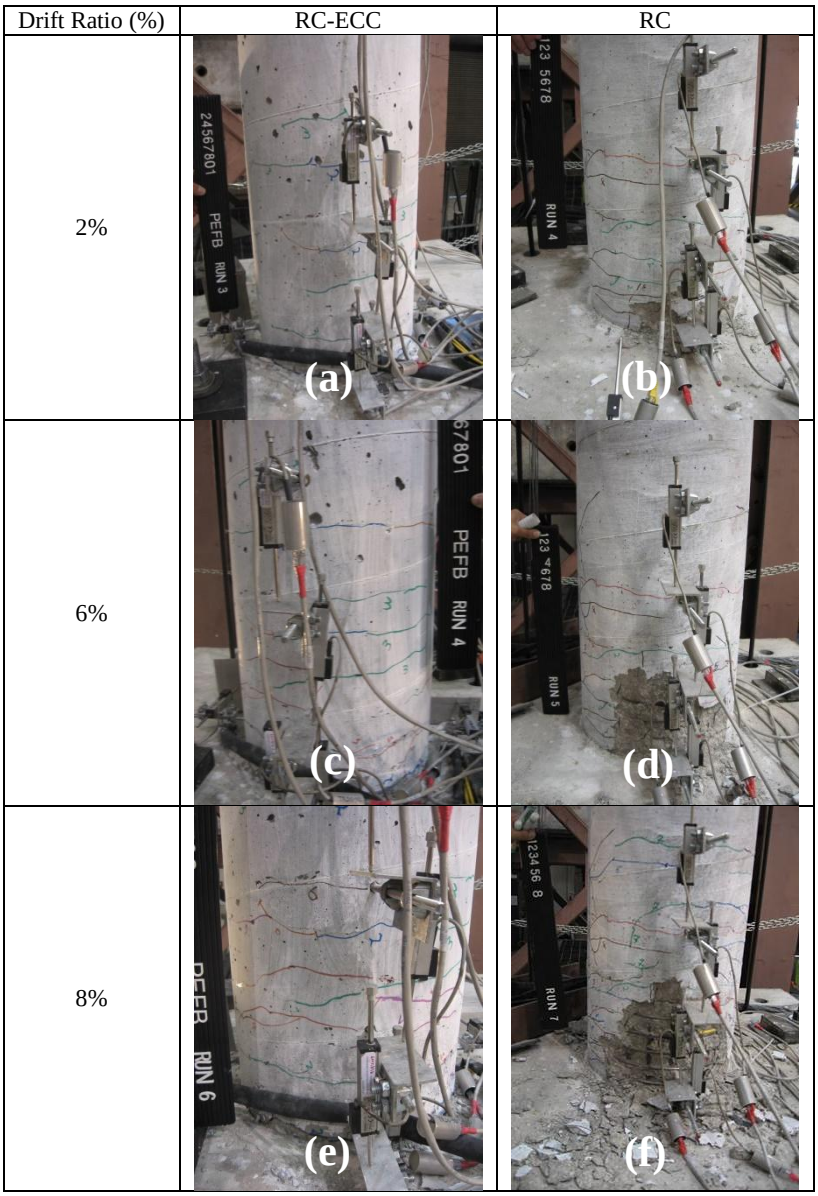

Figure 16. Apparent damage at approximately 2%,6%, and 8% Drift Ratio in RC and RC-ECC column

A detailed OpenSEES [29] model for the two-column pier specimen was developed. The model was a two-dimensional representation of the test bent for in-plane dynamic analysis using a 5% damping ratio, which was within the measured ratio of 2 to 9%. A damping ratio in range of 3% to 5% is recommended for a reinforced concrete structure by most building codes ([30]).

The column sections were defined with a fiber model using measured material properties of the test columns. The schematic of the analytical model is shown in *Fig. 17*. A nonlinear rotational spring was assumed at the column bases to take bond-slip rotations into account using a method developed by Wehbe, et al., ([31]). The bond-slip spring was modeled by a tri-linear "uniaxialMaterial Hysteretic" material composed of the bilinear idealized curve followed by an extension branch with zero stiffness. It should be noted that the spring properties are identical in the positive and negative directions because the column sections are symmetric ([32]).

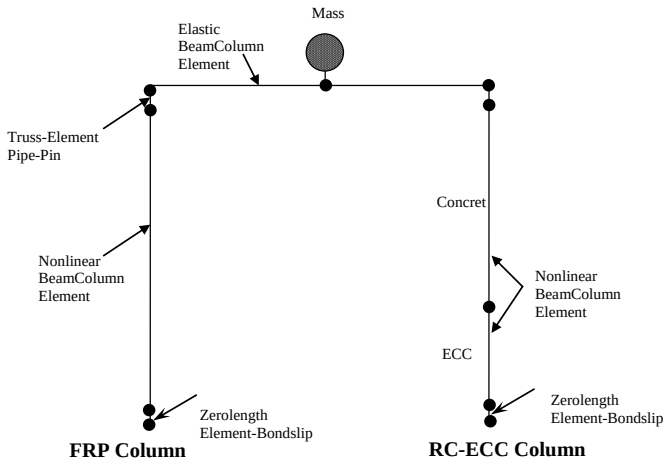

Figure 17. Schematic analytical model of PEFB

The mass was lumped at a node in the middle of the beam. The measured axial load history was applied to the bent model during the analysis.

Two sections were defined for RC-ECC, one for the zone that incorporated ECC and the other for concrete. The confinement model developed by Motaref et al., ([22]) was used for the confined part of ECC. The CFFT section included the FRP tube material in the cover and confined concrete in the core. The Saiidi's confinement model [33] was used to determine the in-fill concrete properties. FRP tube was defined using a modified model of FRP material that was initially proposed by Zhu, ([4]). *Figure 18* shows the modified FRP material stress-strain graph.

Nonlinear beam column elements were used to model columns. CFFT was modeled with one element and a total of seven integration points. RC-ECC was modeled with two elements consisting of the ECC part with three integration points and the concrete part with five integration points.

The pipe pins were designed to remain elastic. Thus, they were modeled using two stiff truss elements on top of the columns to allow for moment-free rotations. The cap beam was modeled using a linear beam element because no

nonlinear deformations were expected.

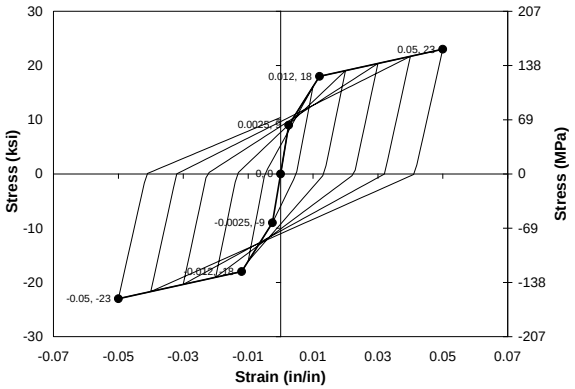

Figure 18. Modified material model for FRP Tube, longitudinal

6.2 Comparison of experimental and analytical results

Pushover analyses and nonlinear dynamic analyses were conducted. Achieved shake table motions for different Runs were spliced and used in dynamic analyses. The measured and calculated force-displacement relationships and displacement histories were superimposed to evaluate the accuracy of the modeling techniques in calculating the nonlinear response of the test bent.

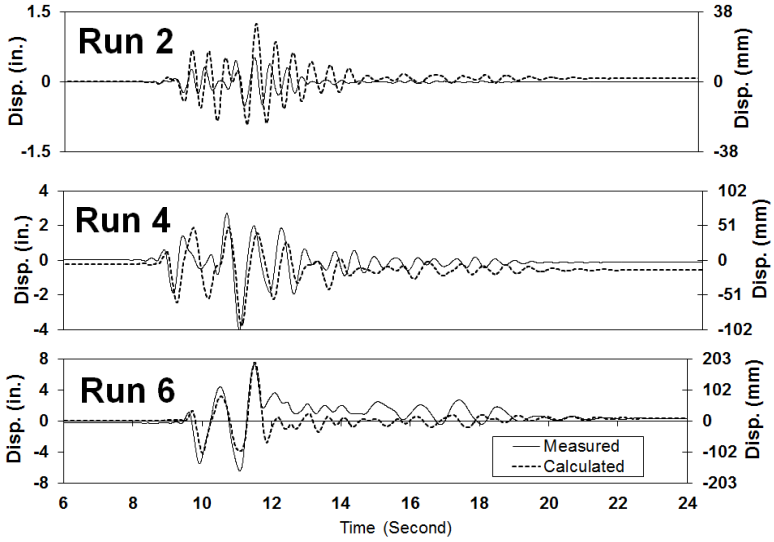

Figure 19. Displacement history of the bent

Figure 19 compares the calculated and measured displacement histories of the bent during a small, medium, and the failure Run (Runs 2, 4, and 6). The

amplitudes of the analytical results were higher than the measured data in Run 2, which could be attributable to underestimation of the hysteretic damping at low amplitudes in the analytical model. The correlation improved as the amplitudes increased, and the hysteretic damping became more dominant in Runs 4 and 6. During these runs the measured and calculated response exhibited close correlation with respect to the amplitudes and waveforms.

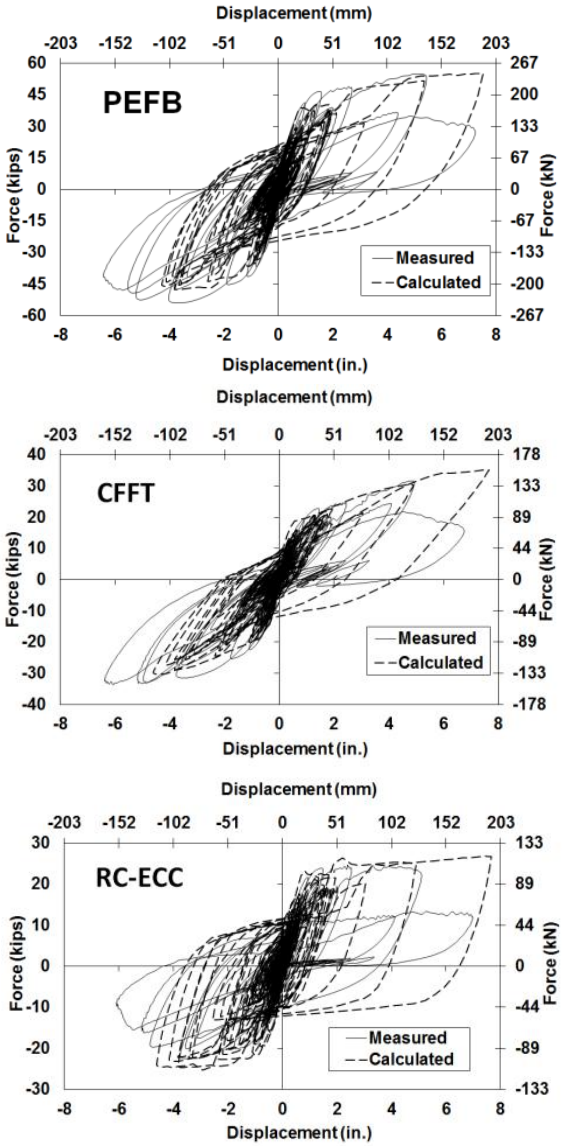

Figure 20. a) Measured and calculated force-displacement of the bent, b) CFFT, c) RC-ECC

Figure 20 compares the analytical and experimental cumulative force-displacement relationships for the bent, RC-ECC, and CFFT. Generally, close agreement was seen between the calculated and measured responses in the positive direction before the last Run. The maximum calculated lateral load capacities of the bent, RC-ECC, and CFFT were 0.4%, 8%, and 11% larger than the maximum measured capacities, respectively. There was a large drop in the lateral load capacity due to the bars rupture, rupture of FRP and ECC spalling during the last run those were not captured by the analytical model. The displacements in the negative direction of motion were underestimated. Overall, the correlation between the measured and calculated results was reasonably close and acceptable.

6.3 Parametric Studies

The effects of FRP tube thickness, FRP tube fiber orientation, and column longitudinal steel reinforcement ratio were studied in CFFT using the analytical modeling method described in the previous section. The basic model for parametric study was a single cantilever column with similar geometry as defined for CFFT previously. A gravity load of 222.4 kN (50 kips) was applied on the column. The reinforcement yield strength of 468.8 MPa (68 ksi) and an unconfined concrete compressive strength of 34.5 MPa (5 ksi) were assumed. The column was analyzed under half cycle loadings with maximum drift ratios of 5%. Cyclic rather than nonlinear response history analysis was conducted to clearly identify the effect of parameters on the response. The analysis was conducted for a drift ratio of 5% because this is the drift level expected under the maximum design earthquake in many bridge columns.

The FRP tube thickness mainly affects the in-fill concrete confinement. Thicker tubes increase confinement and the concrete compressive strength and ductility. *Figure 21(a)* shows the force-displacement response of columns with different FRP tube thicknesses. The initial stiffness in all cases was similar, but the maximum lateral load capacities increased for thicker tubes. The residual displacement upon unloading (the displacement when the column is unloaded to zero force) was insensitive to the tube thickness.

The force-displacement response of CFFT with different fiber orientations is shown in *Fig. 21(b)*. The fiber angle is measured between the fiber and the column axes. The fiber angle affects both the longitudinal and hoop properties of FRP tube. The lateral load capacity was the highest when the fiber orientation was $\pm 35^{\circ}$. This is because smaller fiber angles lead to larger component of fiber stresses in the longitudinal direction. The smaller fiber angle, of course, reduces confinement and the concrete strength. However, *Fig. 21(b)* shows that the higher contribution of fibers in the longitudinal direction had a more dominating effect. The results also show that the residual displacement decreased with lower fiber angles. The larger role of the tube in resisting lateral

forces translates into smaller reinforcing steel strains and lower steel residual strains. The lower steel residual strains translate into smaller overall column residual displacements.

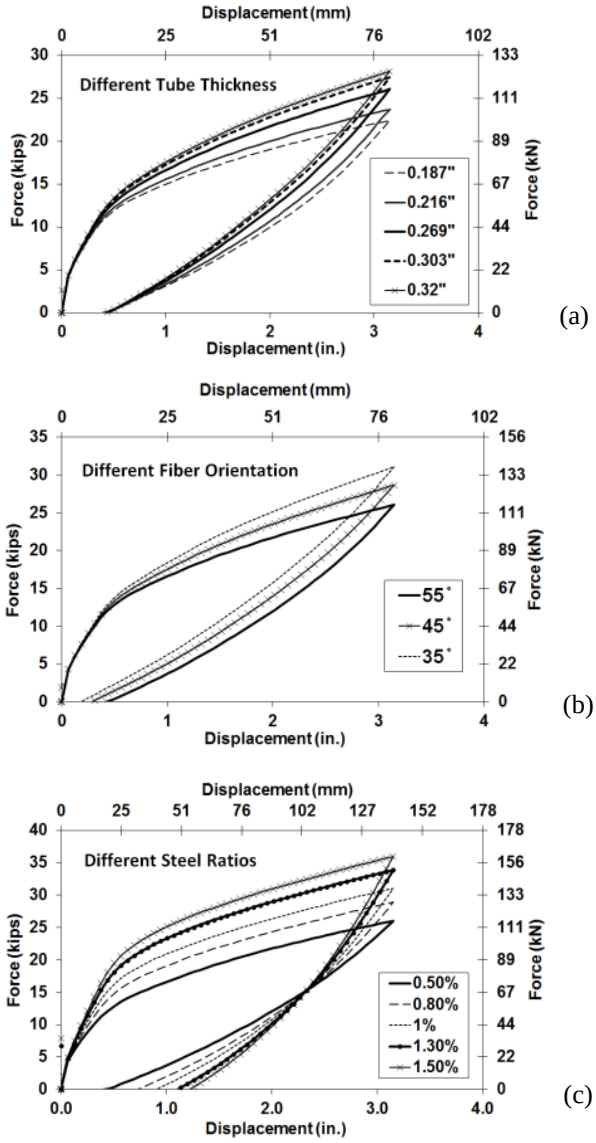

Figure 21. Parametric study results

The force-displacement response of columns with different steel ratios is shown in *Fig. 21(c)*. The longitudinal steel ratio in the basic model was 0.5%. Larger

amount of longitudinal steel reinforcement in the column increased the lateral load capacities, as expected. The maximum lateral load capacity of the column incorporating 1.5% longitudinal steel ratio was 38% larger than that of the basic model (0.5% steel ratio) for loading to 5% drift ratio. As the role of reinforcing steel increased, the residual steel strains and residual column displacements also increased as shown in *Fig. 21(c)*.

7 CONCLUSIONS

The following observations and conclusions present the highlights of this study:

- The accelerated bridge construction technique utilizing precast elements and the connections used in this study led to an earthquake-resistant bent system with excellent performance. The overall seismic response indicated that full column moments were developed similar to that expected of monolithic connections. The element and connection details are recommended for application in ABC.
- Minimal ECC spalling was observed even under 8.6% drift ratio in the precast column incorporating ECC in the plastic hinge. Due to ductile behavior of ECC, spalling was minor and it was limited to a small area. Incorporating ECC in column plastic hinges is recommended to improve resiliency of highway bridges.
- No apparent damage was detected in the plastic hinge zone of CFFT before tensile rupture of the FRP tube under 11.5% drift ratio. Longitudinal steel bars buckled only after FRP tube ruptured. CFFT presents a viable alternative for ABC with improved resiliency of bridge columns.
- The hardening effect after yielding was substantially more significant in CFFT compared to RC-ECC due to the fact that the FRP tube remained elastic while the steel reinforcing bars in RC-ECC yielded.
- Under the same displacement amplitude and when the column lateral strengths are comparable, energy dissipation in a reinforced concrete member is higher than that of a CFFT because the hysteresis loops in the latter are narrower due to smaller residual displacements.
- The embedment length of 1.5 times the column diameter in the footing was sufficient to provide full fixity at the base in both RC-ECC and CFFT.
- The analytical results for PEFB reasonably matched the experimental results. This suggests that existing analytical tools are sufficient in modeling the seismic performance of bridges with advanced details of the type used in this study.
- Concrete-filled FRP tube columns incorporating a minimum amount of longitudinal steel are ductile and appropriate for use in earthquake-resistant CIP or precast bridge columns.
- The experimental results demonstrated that the plastic hinge length is longer in the CFFT compared to the RC-ECC. Distribution of yielding in lower

part of CFFT was over a larger portion of the column length. This results in larger spread of plasticity and reduces the local strain demand on the material.

- Steel pipe pins are recommended for use in accelerated bridge construction because of their ease of construction and effectiveness in eliminating moment transfer.

ACKNOWLEDGEMENTS

The research presented in this paper was funded by the California Department of Transportation under Contract No. 59A0591. The advice, comments, and support of the Caltrans project manager, Dr. Li-Hong Sheng are much appreciated. The authors would like to acknowledge the Fiber Glass Systems for donating the FRP tube used in the two-column bent, and ERICO Company for donation of Lenton Terminators. The authors would also like to thank Dr. P. Laplace, P. Lucas, C. Lyttle, A. Taheri, and J. Cushman for their help in constructing and testing the column models.

REFERENCES

[1] Khaleghi, B, "Use of Precast Concrete Members for Accelerated Bridge Construction in Washington State", Transportation Research Record: Journal of the Transportation Research Board, CD 11-S, Transportation Research Board of the National Academies, Washington, D.C., p. 187–196, 2005.

[2] Hieber, DG, Wacker, JM, Eberhard, M, Stanton, JF, "Precast Concrete Pier Systems for Rapid Construction of Bridges in Seismic Regions, Final Technical Report", Washington State Transportation Center (TRAC), University of Washington and Washington State Department of Transportation, 2005.

[3] Mirmiran, A, Naguib, W, and Shahawy, M, "Principles and analysis of concrete-filled composite tubes", J. Adv. Mater., 32(4), p. 16–23, 2000.

[4] Zhu, Z, "Joint Construction and Seismic Performance of Concrete-Filled Fiber Reinforced Polymer Tubes", Ph.D. dissertation, North Carolina State University, Raleigh, North Carolina, 2004.

[5] Shao, Y, "Seismic performance of FRP-concrete beam-column", Ph.D. dissertation, North Carolina State University, Raleigh, North Carolina, 2003.

[6] Zaghi, AE, Saiidi, M, and Mirmiran, A, "Shake table response and analysis of a concrete-filled FRP tube bridge column", Composite Structures, Elsevier, Volume 94, Issue 5, p. 1564–1574, April 2012.

[7] Li, VC, "Engineered Cementitious Composites – Tailored Composites Through Micromechanical Modeling, in Fiber Reinforced Concrete: Present and the Future", N. Banthia, A. Bentur, and A. Mufti (eds), Canadian Soc. for Civ. Engrg., Montreal, p. 64-97, 1998.

[8] Billington, SL, Yoon, JK, "Cyclic Response of Precast Bridge Columns with Ductile Fiber-reinforced Concrete", ASCE J. Bridge Engineering;. 4 (9):, p. 353-363, 2004.

[9] Saiidi, M, O'Brien M, Zadeh M, "Cyclic Response of Concrete Bridge Columns Using Superelastic Nitinol and Bendable Concrete", American Concrete Institute, ACI Structural Journal, Vol. 106, No. 1, p. 69-77, January-February 2009.

[10] Li, VC, Kabele, HP, Kanda, T, Lim, YM, "Repair and retrofit with engineered cementitious composites", Journal of Engineering Fracture Mechanics; 65(3), 317-334, 2000.

[11] Marcakis, K, Mitchell, D, "Precast concrete connections with embedded steel members", PCI Journal, V.25, No.4, July-August 1980, p.88-116, 1980.
[12] Pertold, J, Xiao, RY, Wald, F, "Embedded steel column bases I. Experiments and numerical simulation", Journal of Constructional Steel Research 56, p. 253–270, 2000a.
[13] Sadeghian, P, Fam, A, "Bond-Slip Analytical Formulation toward Optimal Embedment of Concrete-Filled Circular FRP Tubes into Concrete Footings", Journal of Engineering Mechanics, ASCE, Vol. 136, No. 4, p. 24-533, 2010.
[14] Zaghi, AE, Saiidi, M, "Bearing and Shear Failure of Pipe-Pin Hinges Subjected to Earthquakes", Journal of Bridge Engineering, ASCE, 16(3), p. 340–350, 2011.
[15] Frosch, RJ, Shear transfer between concrete elements using steel pipe connection. ACI Struct. J., 96(6), p. 1003–1008, 1999.
[16] Restrepo, JI, Panagiotou, M, "BART aerial guideway shear key tests, Dept. of Structural Engineering", Univ. of California, San Diego, 2005.
[17] California Dept. of Transportation. "Memos to designers, Division of Engineering Services", Sacramento, CA, 2008.
[18] Roberts, JE, "Caltrans structural control for bridges in highseismic zones" Earthquake Eng. Struct. Dyn., 34(4–5), p. 449–470, 2005.
[19] Hipley, P, "Bridge retrofit construction techniques", Second National Seismic Conf. on Bridges and Highways, Sacramento, CA, 1997.
[20] Paulay, T, Priestley, MJN, "Seismic Design of Reinforced Concrete and Masonry Buildings", Wiley Interscinece, 1992.
[21] Shao, Y, Mirmiran, A, "Experimental Investigation of Cyclic Behavior of Concrete-Filled Fiber Reinforced Polymer Tubes", J. Compos. Constr., 9(3), p. 263–273, 2005.
[22] Motaref, S, Saiidi, M, and Sanders, D, "Seismic response of precast bridge columns with energy dissipating joints", Center for Civil Engineering Earthquake Research, Department of Civil and Environmental Engineering, University of Nevada, Reno, Nevada, Report No. CCEER-11-01, 2011.
[23] California Department of Transportation. Seismic Design Criteria (SDC), Division of engineering services, Sacramento, California, 2006.
[24] Pertold, J, Xiao, RY, Wald, F, "Embedded steel column bases II. Design Model Proposal", Journal of Constructional Steel Research 56, p. 271–286, 2000 b.
[25] Zaghi, AE, Saiidi, M, El-Azazi, S, "Shake Table Evaluation of a Two-Column Bridge Bent Model Incorporating Pipe-Pin Hinges", Journal of Bridge Engineering, ASCE, Vol. 16, No. 5, 2011.
[26] Kawashima, K, MacRae, GA, Hoshikuma, J, Nagaya, K, "Residual displacement response spectrum", Journal of Structural Engineering, 124(5), p. 523-530, 1998.
[27] Zaghi, AE, Saiidi, M, "Seismic design of pipe-pin connections in concrete bridges", Rep. No. CCEER-10-01, Center for Civil Engineering Earthquake Research, Dept. of Civil and Environmental Engineering, Univ. of Nevada, Reno, NV, 2010.
[28] Zhu, Z, Mirmiran, A, Saiidi, MS, "Seismic Performance of Fiber Composite Tubed Reinforced Concrete Bridge Substructure", Transportation Research Record No. 1976, Design of Structures, Part 7 – Structural Fiber Reinforced Plastics, Transportation Research Board, National Research Council, Washington, D.C., p. 197-206, 2006.
[29] Mazzoni, S, McKenna, F, Scott, MH, Fenves, GL, "OpenSEES Command Language Manual", Berkeley, CA, 2007.
[30] Chopra, AK, "Dynamics of Structures (3rd Edition)", Prentice Hall, New Jersey, 2006.
[31] Wehbe, N, Saiidi, M, Sanders, D, "Seismic Performance of Rectangular Bridge Columns with Moderate Confinement", American Concrete Institute, ACI Structural Journal, Vol. 96, No. 2, p. 248-259, 1999.
[32] Vosooghi, A, Saiidi M, "Design Guidelines for Rapid Repair of Earthquake-Damaged Circular RC Bridge Columns Using CFRP", Journal of Bridge Engineering, ASCE, Vol. 18, No. 9, p. 827-836, September 2013.

[33] Saiidi, M, Sureshkumar K, Pulido C, "Simple Carbon-Fiber-Reinforced-Plastic-Confined Concrete Model for Moment-Curvature Analysis", Journal of Composites for Construction, ASCE, Vol. 9, No. 1, January-February p. 101-104, 2005.